Microvascular Alterations in Diabetic Mice Correlate With Level of Hyperglycemia

Petra Algenstaedt,[1] Christian Schaefer,[2,3] Tanja Biermann,[3] Andreas Hamann,[4] Britta Schwarzloh,[1] Heiner Greten,[1] Wolfgang Rüther,[2,3] and Nils Hansen-Algenstaedt[2,3]

Vascular alterations are the most common causes of morbidity and mortality in diabetic patients. Despite the impact of endothelial dysfunction on microcirculatory properties, little is known about the endothelial cell alteration during the development of diabetes and its correlation to the metabolic situation. For that reason we continuously monitored in vivo functional and morphological alterations of the microvasculature in hyperglycemic and hyperinsulinemic transgenic UCP1/DTA mice with brown fat deficiency, using a dorsal skin-fold chamber preparation and fluorescence microscopy. UCP1/DTA mice showed a dramatic decrease in vascular density due to a remarkable reduction of small vessels. Vascular permeability and leukocyte endothelial interactions (LEIs) significantly increased. The extent of vascular alteration correlated with the extent of metabolic dysfunction. Decreased tissue perfusion observed in UCP1/DTA mice might play a role in impaired wound healing observed in diabetes. The increased permeability in subcutaneous tissue may serve as predictor of vascular changes in early stages of diabetes. The increased LEI and serum tumor necrosis factor-α levels, which mirror the inflammatory process, support the growing evidence of the inflammatory component of diabetic disease. The results suggest that anti-inflammatory strategies might be able to prevent vascular deterioration in early stages of diabetes. Further investigations are required to evaluate the benefit of such therapeutic strategies. *Diabetes* 52:542–549, 2003

Vascular alterations are the most common causes of morbidity and mortality in diabetic patients. The microcirculation not only governs the efficacy of substrate delivery but also mediates adaptations to changing local requirements and metabolic conditions. Functional alterations of the microcirculation precede morphological changes and determine the resultant vascular morphology (1). Microvascular disease has been shown to have a high prevalence in diabetes (2,3). Several studies described endothelial dysfunction and functional alterations in the microcirculation of diabetic patients. Animal models of diabetes show increased vascular permeability (4), alterations in erythrocyte velocity (5), sequestration of leukocytes in the microcirculation (5–7), and morphological alterations such as altered vascular density (5). These alterations are mainly described as the result of hyperglycemia and advanced glycation end products (8,9) and develop sequentially. Functional alterations, such as increased microvascular permeability and increased entrapment of leukocytes, have been described as an early event in diabetes and in animal models and could be partially observed after only a few hours of hyperglycemia (4,7). Morphological alterations, such as altered microvascular density and diameter, appear later (5,10). However, mechanisms that lead to microangiopathies in diabetic patients remain only partially understood.

Monitoring of microcirculatory alterations in patients is limited by the invasive character of methodology and is limited to ophtalmoscopic and postmortal histology. It is therefore important to investigate the sequential alteration of the microcirculation in diabetes with methods allowing continuous monitoring of animal models, which mimic the sequential metabolic alterations in diabetic disease. In our study, we used UCP1/DTA mice characterized by severe brown fat deficiency with a consecutive reduction of energy expenditure (11). As animals age, they develop marked obesity, insulin resistance, hyperglycemia, hyperlipidemia, leptin resistance, and hypertension, thus resembling the complete metabolic syndrome of obese humans (12–14). In light of previous findings, the goal of the present study was to identify potential therapeutic interventions by discerning the sequential step in vascular deterioration.

RESEARCH DESIGN AND METHODS

Diabetic model. Transgenic mice expressing diphteria toxin A chain (DTA) regulated by the uncoupling-protein gene-promotor (UCP promoter) selectively in brown adipose tissue (11) were used. UCP1/DTA mice develop severe brown adipose tissue deficiency leading to decreased energy expenditure. They are characterized by hyperphagia beginning at 8 weeks, which is followed by obesity, hyperglycemia, and hyperinsulinemia (11). An average increase of 54% (male mice)/75% (female mice) in

From the [1]Department of Internal Medicine, University Hospital Hamburg-Eppendorf, Hamburg, Germany; the [2]Department of Orthopedic Surgery, University Hospital Hamburg-Eppendorf, Hamburg, Germany; the [3]Center of Biomechanics, University Hospital Hamburg-Eppendorf, Hamburg, Germany; and the [4]Department of Internal Medicine I, University Hospital Heidelberg, Heidelberg, Germany

Address correspondence and reprint requests to Nils Hansen-Algenstaedt, Department of Orthopaedic Surgery, University Hospital Hamburg-Eppendorf Martinistr 52, 20246 Hamburg, Germany. E-mail: nhansen@uke.uni-hamburg.de.

Received for publication 30 July 2002 and accepted in revised form 12 November 2002.

BFR, blood flow rate; CCD, charge coupled device; DTA, diphteria toxin A chain; FITC, fluorescein isothiocyanate; GTT, glucose tolerance test; HT, hematocrit; ICAM, intracellular adhesion molecule; LEI, leukocyte endothelial interaction; TNF, tumor necrosis factor; TRITC, tetramethylrhodamine; UCP promoter, uncoupling-protein gene-promotor; VCAM, vascular cell adhesion molecule; VD, vascular density.

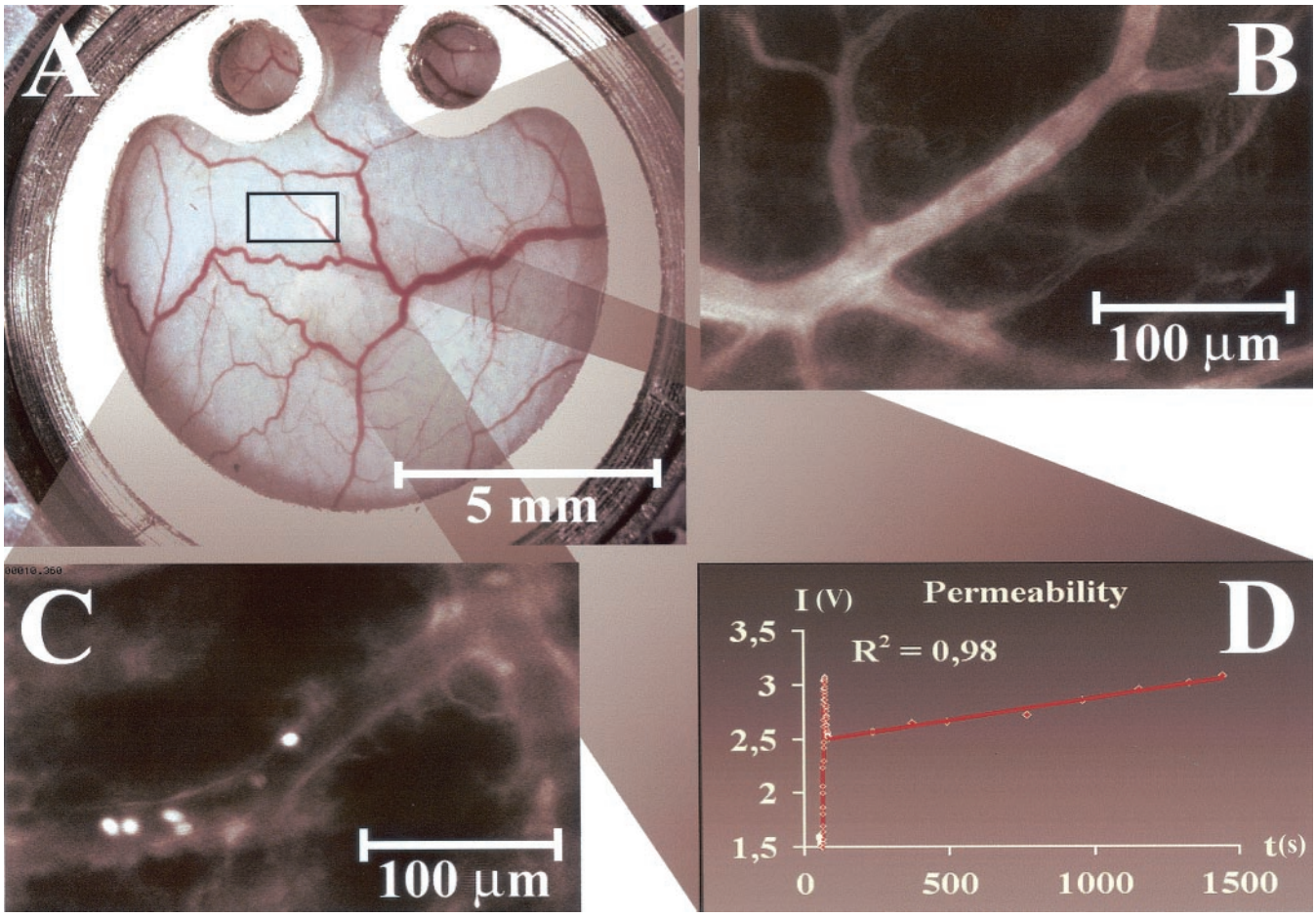

FIG. 1. Intravital microscopy. *A*: Digital photo of dorsal skin-fold chamber preparation at day 0, showing subcutaneous microcirculation. *B*: Image of microcirculation after intravenous application of FITC-Dextran as plasma tracer for measurements of VD, diameter, and blood flow. *C*: Image of microcirculation after in vivo labeling of leukocytes with Rho-6G for measurement of LEIs. *D*: Fluorescence intensity I(V) of extravasating fluorochrome plotted against time t(s) for measurements of microvascular permeability in UCP1/DTA mice. The slope of the graph is related to the microvascular permeability.

body weight, 30% in blood glucose levels, and an 85- to 125-fold increase in blood insulin levels at the age of 22 weeks (14,15) have been documented in UCP1/DTA mice. To mimic early-stage diabetes, mice at the age of 20 weeks with established obesity and hyperglycemia were used in this study. Nontransgenic littermates were used as controls. Mice were caged individually at 24°C and 50% humidity and fed with standard rodent chow (Chow no. S5714S040; Ssniff, Soest, Germany) and water ad libitum. All animal procedures were performed according to the German animal welfare committee.

Blood glucose, temperature, glucose tolerance test, and tumor necrosis factor-α. Body weight, body temperature, and whole blood glucose levels were measured 2 days before dorsal skin-fold chamber implantation, on the day of the surgical procedures, and 6 and 9 days after implantation. A glucose tolerance test (GTT) was performed on the day of chamber implantation by injecting a 10% glucose solution (1 mg glucose/g body wt) intraperitoneally after an overnight fast (12 h). Blood was collected with a heparinized capillary, and whole blood glucose was measured 0, 15, 30, 60, 90, and 120 min after glucose injection via the glucose oxidase method (One Touch, Life Scan, Milpitas, CA). Serum levels of tumor necrosis factor (TNF)-α were determined using an immunoassay (Mouse TNF-a, Quantikine M; R&D Systems, Minneapolis, MN). Blood was collected by heart puncture with a heparinized syringe.

Dorsal skin-fold chamber preparation. To noninvasively and continuously measure microcirculatory parameters, we implanted a dorsal skin-fold chamber as previously described (16,17) (Fig. 1*A*). Before surgical procedures, mice were anesthetized (7.5 mg ketamine hydrochlorid and 2.5 mg xylazine/100 g body wt) and their skin was shaved and depilated. Dorsal skin-fold chambers (weight 3.2 g; Machine shop, Boston, MA) were implanted exposing subcutaneous tissue and striated skin muscle as described previously (16). All surgical procedures were performed at aseptic conditions while maintaining body temperature at physiological levels. The mice were allowed to recover for 6 days.

Intravital microscopy. To obtain microcirculatory parameters, randomly selected areas (four to five locations) were investigated using a fluorescence microscope (Axioplan; Zeiss, Oberkochen, Germany). The microscope is equipped with filter sets for fluorescein isothiocyanate (FITC) and tetramethylrhodamine (TRITC), a 20× objective lens (LD Achroplan 20×/0.40; Zeiss, Germany), an intensified charge coupled device (CCD) video camera (C2400–97; Hamamatsu Photonics, Germany), a Photomul-

tiplier Tube (R4632; Hamamatsu Photonics, Herrschingam Ammersee, Germany), and a computer (Apple Power MacIntosh).

Functional vascular density and blood flow rate. A total of 100 μl FITC labeled Dextran (MW 2,000,000, 50 mg/ml 0.9% saline; Sigma, St. Louis, MO) was injected through the tail vein to visualize blood vessels. During each observation period, FITC images were recorded for 30 s and analyzed off-line (Fig. 1*B*). The erythrocyte velocity (V_{RBC}) was measured opto-electronically using a two-slit method and an image processing system (Exbem 3.0; Pixlock e.k., Münster, Germany; National Institutes of Health Image 1.62) as described elsewhere (18). The mean blood flow rates (BFRs) of individual vessels were calculated using diameter (D) and V_{mean}.

BFR = $\pi/4 \times V_{mean} \times D^2$, where $V_{mean} = V_{RBC}/\alpha$ (α = 1.3, for blood vessels <10 μm; linear extrapolation $1.3 < \alpha < 1.6$ for blood vessels between 10 and 15 μm; and $\alpha = 1.6$ for blood vessels >15 μm) (19). The functional vascular density (VD), defined as the total length of functional vessels per unit area (measured in centimeters per centimeters squared) and the vessel diameter were analyzed using an image processing system (National Institutes of Health Image 1.62), as described elsewhere (16,18).

Vascular permeability. Effective microvascular permeability (P) was measured as described previously (17,20). After the injection of TRITC-labeled BSA (TRITC-BSA, MW 67,000; Molecular Probes, Eugene, OR) (10 mg/ml, 0.1 ml/25 g body wt), the fluorescence intensity was measured intermittently for 25 min and recorded digitally (PowerLab/200 ADInstruments; Ply, Castle Hill, Australia) (Fig. 1*D*). The value of P was calculated as $P = (1 - HT)\ V/S\ [1/(I_0 - I_b) \times dI/dt + 1/K]$, where I is the average fluorescence intensity of the whole image, I_0 is the value of I immediately after the filling of all vessels by TRITC-BSA, I_b is the background fluorescence intensity, and HT is the amount of hematocrit. The average HT of vessels is assumed to be equal to 19% (21). V and S are the total volume and surface area, respectively, of vessels within the tissue volume covered by the surface image, respectively. The time constant of BSA plasma clearance (K) is 9.1×10^3s (22).

Leukocyte endothelial interactions. Leukocyte-endothelial interactions (LEIs) in vessels were monitored as described previously (23). Mice were injected intravenously with a bolus (20 μl) of 0.1% rhodamine-6G in 0.9% saline, and leukocytes were visualized via an intensified CCD camera and recorded noncompressed digitally on a computer (Apple Power MacIntosh) (Fig. 1*C*). The numbers of rolling (Nr) and adhering (Na) leukocytes were counted for 30 s along a 100-μm segment of a vessel. Rolling was defined as a slow movement along the vessel wall (<50% of V_{RBC}), and adhering was defined as a stable position at the vessel wall for 30 s. The total flux of cells for 30 s was measured (Nt). The total leukocyte flux was normalized by the cross-sectional area of the individual vessel. Leukocyte flux (measured in cells per millimeters squared) = $10^6 \times Nt/(\pi \times [D/2]^2 \times 30s)$. Rolling count, the ratio of rolling leukocytes (Nr) to total cell flux (Nt) was calculated as follows: rolling count (%) = 100 × Nr/Nt. The mean leukocyte adhesion at the vessel wall was calculated by normalizing the vessel surface area. Adhesion density (measured in cells per millimeters squared) = $10^6 \times Na/(\pi \times D \times 100\ \mu m)$. Shear rate of individual blood vessels was calculated according to the following equation: shear rate (s^{-1}) = $8 \times V_{mean}/D$ (23).

Statistics. Results are presented as the mean ± SE of the mean. Values of the transgenic versus control group were compared with the Mann-Whitney test using StatView (Abacus, Berkeley, CA). To test correlations between parameters, *t* tests for Spearman's rank correlation were performed and groups were compared with the Mann-Whitney test. *P* values <5% were considered to be significant.

RESULTS

Body temperature. Significantly lower body temperature of UCP1/DTA mice (~1°C; data not shown) corroborate observations of reduced body temperature from previous studies (15). Overnight fast caused a decrease in body temperature of the controls, whereas no extra decrease in body temperature of UCP1/DTA mice was observed.

Body weight. Compared with controls, body weight of UCP1/DTA mice increased significantly (52.5%), as described previously (14) (data not shown). The difference in body weight between UCP1/DTA mice and controls decreased from day 0 (52.5%) to day 9 (32.3%) due to a more pronounced loss in body weight in the transgenic group (−18.2%) compared with the control group (–5.7%). The initial loss in body weight (5%) was probably due to the overnight fast, whereas the further loss might be related to the chamber implantation. A 15% loss in body weight has been reported after dorsal skin-fold chamber implantation (16). Analysis revealed a significant correlation of weight loss (day 0 – day 9) with the body weight at day 0 independently of group (data not shown).

Blood glucose and glucose tolerance test. We measured blood glucose at day −2, 0, 6, and 9 (Fig. 2*A*). UCP1/DTA mice showed significant elevated glucose levels throughout the whole observation period. Compared with the control group (107 ± 3 vs. 109 ± 3 mg/dl), an increase to 206 ± 13 mg/dl (+92.1%, day 6) and 195 ± 13 mg/dl (77.9%, day 9) was measured. Additionally, a glucose tolerance test (GTT) was performed (Fig. 2*B*). The blood glucose after an overnight fast was 151.4 mg/dl (mean ± 9.1) in UCP1/DTA mice, indicating the diabetic state, whereas controls showed physiological fasting glucose (81.4 ± 4.2 mg/dl). GTT was significantly elevated in UCP1/DTA mice compared with controls.

Microcirculatory parameters

Permeability. The microvascular permeability (P) was significantly higher ($22 \times 10^{-7} \pm 2.3 \times 10^{-7}$cm/s) in UCP1/DTA mice than in controls ($6.2 \times 10^{-7} \pm 4.2 \times 10^{-7}$ cm/s) (Fig. 2*C*).

Functional vessel density and diameter. Analysis of functional VD revealed a significant decrease in UCP1/DTA mice (day 6, 264 ± 11 cm/cm^2 and day 9, 276 ± 13 cm/cm^2) compared with control mice (day 6, 326 ± 9cm/cm^2 and day 9, 323 ± 9 cm/cm^2) (Fig. 3*A*). VD showed a significant negative correlation to the blood glucose level (Fig. 4*B*) and body weight (data not shown). A reduction in VD of 27% was found in the group with blood glucose levels 250–299 mg/dl (246 ± 11 cm/cm^2) compared with the group with blood glucose levels 50–99 mg/dl (335 ± 12

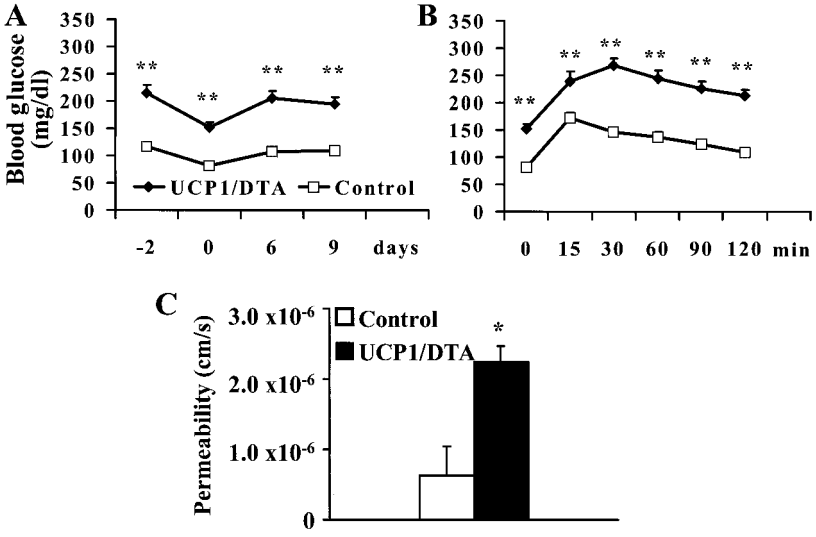

FIG. 2. ***A*****: Blood glucose levels in UCP1/DTA (*n* = 14) and controls (*n* = 18) were measured at day –2, day 0, day 6, and day 9 after dorsal skin-fold chamber preparation.** ***B*****: Glucose tolerance test in UCP1/DTA (*n* = 14) and controls (*n* = 18) at day 0 before dorsal-skin fold chamber preparation. After overnight fast (12 h), a 10% glucose solution (1 mg glucose/g body wt) was administered intraperitoneally and blood glucose measured at indicated time points.** ***C*****: Microvascular permeability in UCP1/DTA (*n* = 10) and controls (*n* = 8) was measured via fluorescence intensity measurements of extravasating fluorochrome after intravenous application of Rhodamin-BSA. All values are presented as mean ± SE (**P* < 0.05, ***P* < 0.01).**

cm/cm^2). Vessel diameter (D) in UCP1/DTA mice (day 6, 10 ± 0.8 μm and day 9, 10 ± 1.1 μm) was significantly increased compared with controls (day 6, 5.3 ± 0.2 μm and day 9, 5.2 ± 0.2 μm) (Fig. 3*B*). Analysis of the vessel diameter distribution illustrated that the diameter peak in control mice (~3 μm) was significantly blunted and shifted to higher values (~2 μm) in UCP1/DTA mice (Fig. 4*A*). Therefore, the increased mean diameter in UCP1/DTA mice was mainly due to a reduction in the number of vessels with diameters ~3 μm. The mean VD was characterized by a positive correlation to blood glucose levels with a plateau phase (9.1 μm) for blood glucose values >160 mg/dl (Fig. 5*A*). A positive correlation between D and body weight was found (data not shown).

BFR and red blood cell velocity. The UCP1/DTA mice showed a significant decrease in blood flow velocity (V_{mean}) (day 6, 529 ± 44 μm/s and day 9, 535 ± 39 μm/s) compared with controls (day 6, 859 ± 46 μm/s and day 9, 818 ± 42 μm/s) (Fig. 5*B*). V_{mean} correlated negatively with blood glucose levels (Fig. 5*A*) and body weight (data not shown) and showed the maximum velocity (840 ± 31 μm/s) at low blood glucose levels (80–119 mg/dl) and a plateau phase (590.7 ± 38.6 μm/s) at high blood glucose levels with values >160 mg/dl. The BFR was found to be unchanged, indicating that the perfusion of vessels is similar in UCP1/DTA mice and controls (Fig. 5*C*).

LEI. Mean diameter of measured venules in control and transgenic mice was 27.1 ± 0.82 and 25.7 ± 1.3 μm, respectively. The rolling count of the transgenic group was significantly higher with 42.4 ± 2.7% on day 6 and 45.2 ± 2.8% on day 9 compared with the control group with 22.0 ± 3.8% on day 6 and 31.1 ± 3.8% on day 9 (Fig. 6*A*). Cell adhesion density was at least threefold higher in the transgenic (day 6, 126 ± 17 cells/mm^2 and day 9, 107 ± 13 cells/mm^2) versus control group (day 6, 39 ± 21 cells/mm^2 and day 9, 13 ± 6 cells/mm^2) (Fig. 6*B*). LEI, leukocyte adhesion density, and the rolling fraction correlated significantly with glucose levels (Fig. 6*C*) and body weight (data not shown). The cell adhesion density of leukocytes correlated positively with the blood glucose level and mirrored the picture of the leukocyte rolling fraction. The leukocyte cell flux per cross-sectional area was significantly lower in transgenic mice (1,830 ± 176 cells/mm^{2}s) compared with controls at day 6 (2,958 ± 375 cells/mm^{2}s) (Fig. 7*A*). A significant reduction in shear rate to 43 and 53% could be found in UCP1/DTA mice (day 6, 185 ± 24^{s-1} and day 9, 210 ± 23^{s-1}) compared with control mice (day 6, 432 ± 37^{s-1}; day 9, 397 ± 40^{s-1}) due to the decreased V_{mean} (Fig. 7*B*). Shear rate correlated significantly with glucose levels and body weight (data not shown) with a strong decrease between 80 and 160 mg/dl blood glucose and a plateau at values >160 mg/dl blood glucose (Fig. 7*C*).

Serum TNF-α. The UCP1/DTA-group showed a significant increase in mean serum TNF-α concentration (9.28 ± 1.60 pg/ml) compared with the control group (3.11 ± 0.87 pg/ml) (Fig. 8*A*). Serum TNF-α levels were found to be significantly correlated to blood glucose levels as well as body weight (data not shown) and had an approximately linear (R^2 = 0.984) increase in dependence of blood glucose (Fig. 8*B*). An increase from 0.69 ± 0.31 to 13.34 ± 3.41 pg/ml at glucose levels of 55–99 and 200–279 mg/dl, respectively, could be measured.

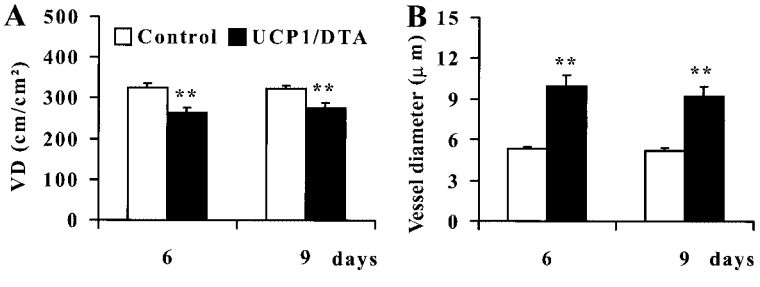

FIG. 3. Functional VD per observation area (*A*) and mean vessel diameter (*B*) was measured in UCP1/DTA (*n* = 14) and controls (*n* = 18) at day 6 and day 9 after dorsal skin-fold chamber implantation. Values are presented as mean ± SE (*P* < 0.01).**

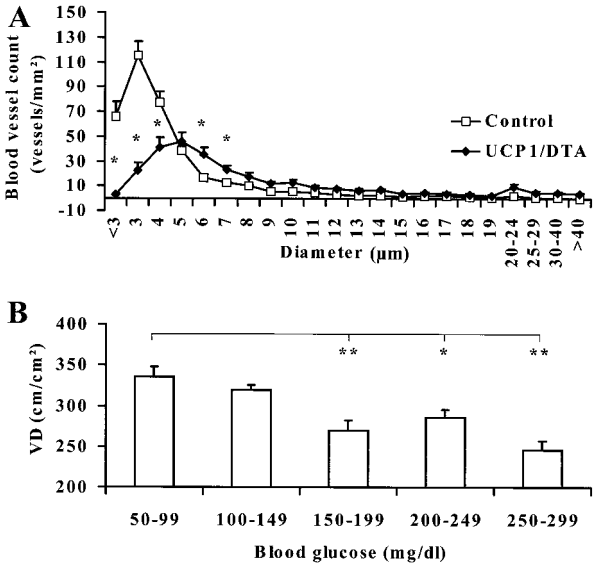

FIG. 4. *A*: **Vessel count per area is plotted against vessel diameter. Vessel diameter peak ~3 μm in control mice was significantly blunted and shifted to higher values (~5 μm) in UCP1/DTA mice (n = 14).** *B*: **VD of all mice (n = 64) and days is plotted against blood glucose values. VD showed a significant negative correlation to the blood glucose level (R^2 = 0.86; P < 0.0001). Values are presented as means ± SE (*P < 0.05, **P < 0.01).**

DISCUSSION

Microcirculatory properties govern the efficacy of substrate delivery, but they also mediate functional and morphological adaptations to local requirements and metabolic conditions. Our results demonstrate for the first time functional and morphological alterations of the microcirculation in early stage diabetic UCP1/DTA mice. We observed that these parameters correlated with the metabolic state represented by blood glucose levels and body weight. Because of the correlations found between the metabolic state and the microcirculatory parameters independently of the group, it is not likely that the microcirculatory dysfunctions are directly due to the animal model.

Increased permeability, especially to albumin, has been shown to be a very early endothelial dysfunction in diabetes in the retina (26), kidney (27), and rat mesentery (5). We showed that increased permeability throughout the subcutaneous tissue, indicating vascular leakage, is an early sensitive parameter of endothelial dysfunction and is observable in early-stage diabetic disease.

VD was decreased in diabetic mice, whereas the vessel diameter was increased as reported earlier (10,28). The combination of an unchanged BFR in blood vessels and a lower VD leads to decreased tissue perfusion in subcutaneous tissue and may therefore lead to an impaired supply of oxygen and nutrients. Analysis of diameter distribution revealed that the decrease in VD and increase in vessel diameter was mainly due to a reduced number of small vessels with diameters between 3 and 5 μm. The failure of small vessels in UCP1/DTA mice might explain impaired wound healing found in diabetic disease. The reduction in VD and increase of vessel diameter correlated with the metabolic situation of the mice represented by the blood glucose levels and body weight. These correlations support the finding that impairment of metabolic control directly leads to progressive morphologic and functional alterations of the microcirculation in early-stage diabetes. The molecular mechanisms of the impaired vessel formation need to be further elucidated. However, there is some evidence that the disturbance in skin vessel stability might be due to altered expression of angiopoetin-1 and -2 and their receptor Tie-2 (29), which are important determinants in vessel maturation, stabilization, and remodelling (30).

The V_{mean} showed a decrease at higher blood glucose levels reaching a plateau at blood glucose levels >160 mg/dl. This is consistent with earlier observations measured in rat mesentery (5) and in conjunctival microcirculation of diabetic patients (28). Surprisingly, the BFR, an important determinant for tissue perfusion, was not changed. The unchanged BFR is likely due to the combination of a lower V_{mean} and the increased diameter.

There is growing evidence that LEI plays an important role in diabetic microangiopathy. Increased LEI have been reported to trigger capillary nonperfusion, blood-retinal barrier breakdown and neovascularization in the eye (24,25), increase ischemia-reperfusion damage (5), and lead to inactivation of nitric oxide (NO) through release of oxigen-derived radicals and therefore to endothelial dys-

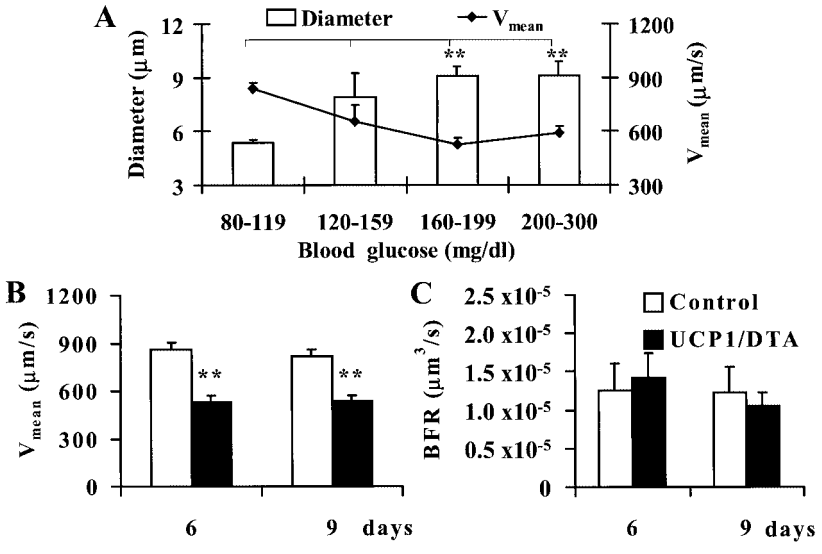

FIG. 5. V_{mean}, BFR, and vessel diameter was measured at day 6 and day 9 after dorsal skin-fold chamber implantation. V_{mean} and vessel diameter of all mice (n = 64) and days is plotted against blood glucose values (*A*). In contrast to the positive correlation of vessel diameter (P < 0.0001), V_{mean} was negatively correlated with blood glucose levels (P < 0.0001). V_{mean} and vessel diameter were characterized by a plateau phase for blood glucose values >160 mg/dl. V_{mean} was significantly reduced in UCP1/DTA (n = 14) compared with controls (n = 18) (*B*), whereas BFR remained unaltered (*C*). Values are presented as mean ± SE (P < 0.01).**

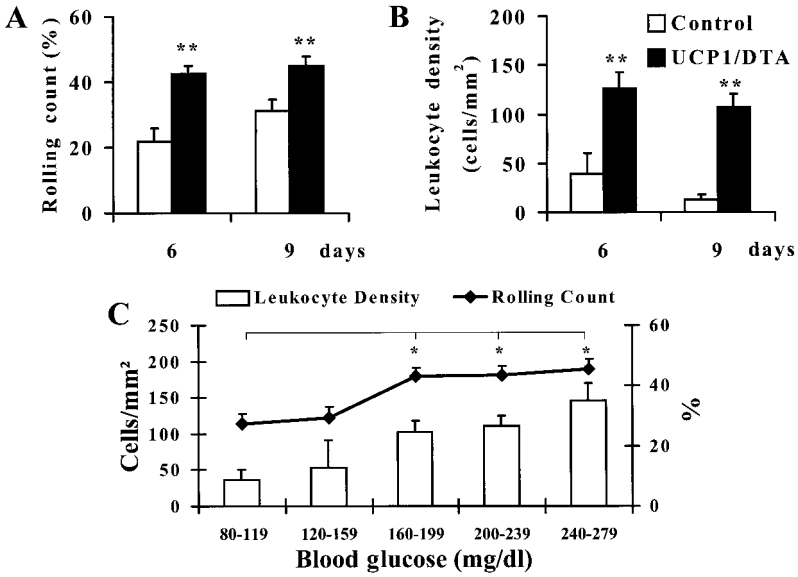

FIG. 6. *A* and *B*: Rolling count and leukocyte density were measured in UCP1/DTA (day 6, n = 12; day 9, n = 11) and controls (n = 9). *C*: Rolling count and leukocyte density at the vessel wall of all mice (n = 41) and days is plotted against blood glucose levels. A positive linear correlation to blood glucose values was found in rolling count (R^2 = 0.85) and leukocyte density (R^2 = 0.96) (P < 0.001). Values are presented as means ± SE (*P < 0.05, **P < 0.01).

function (31). LEIs are mediated by forces of adhesion and blood velocity. Adhesion is determined by the expression of adhesion molecules on the endothelial surface (intracellular adhesion molecule [ICAM]-1, P-selectin, platelet endothelial cell adhesion molecule [PECAM]-1, and vascular cell adhesion molecule [VCAM]-1) (32–35) and the surface of leukocytes (e.g., L-selectin) (33,36). Leukocytes interact with the endothelium by first rolling along the vessel wall, then activating β_2-Integrins expression (32,33), and finally stable binding with possible extravasation thereafter. Counteracting this process is the blood flow (shear rate), which depends on blood flow velocity and vessel diameter. We found significantly increased LEI, leukocyte rolling fraction, and leukocyte density at the vessel wall, which were positively correlated to blood glucose levels and body weight, indicating an inflammatory reaction in the microcirculation induced by impaired metabolic control. These results agree with previous in vivo and in vitro observations of LEI in streptozotocin-induced diabetes in rat mesentery (5), rats given a continuous intravenous glucose infusion (37), and human umbilical vein endothelial cell (HUVEC) in a flow chamber (38). A significantly decreased shear rate indicates that the increased LEI is likely in part due to the reduction of hemodynamic forces in the microcirculation, as described for the mesentery of streptozotocin-induced diabetes of rats (5). But despite the reduction of hemodynamic forces, analysis of correlation of LEI and shear rate with blood glucose levels revealed that shear rate showed a plateau phase at blood glucose levels >160 mg/dl, whereas LEI, rolling count, and leukocyte density, were approximately linearly (R^2 = 0.96) correlated to blood glucose. Therefore, it is not likely that the increased leukocyte adhesion at higher blood glucose values is only due to the lowered shear rate, as discussed previously (5). This conclusion is additionally supported by in vivo observations showing that local application of glucose to nondiabetic rat mesentery led to an increase of LEI without altering shear rate over 12 h (34). Therefore, other influencing factors, such as glucose-induced expression of cell adhesion molecules, might be an explanation for the increased LEI. TNF-α is known to upregulate adhesion molecules (E-selectin,

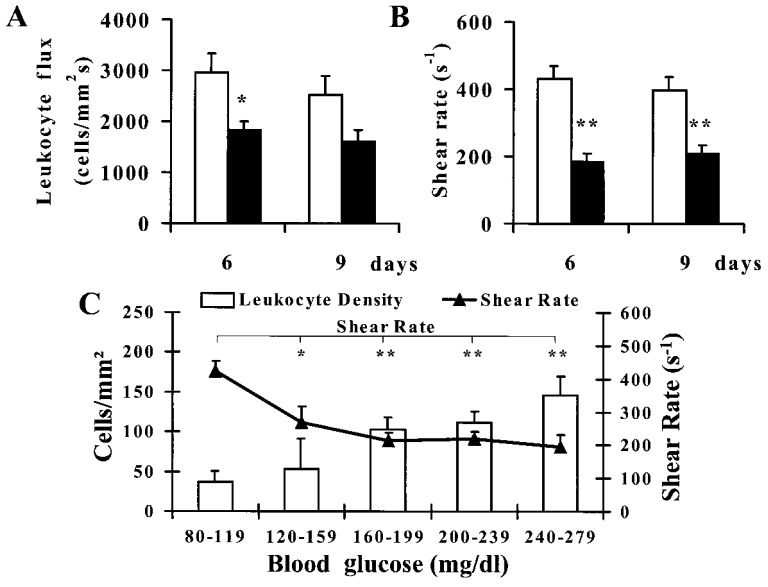

FIG. 7. *A*: Leukocyte flux per cross sectional area in UCP1/DTA (day 6, n = 12; day 9, n = 11) and controls (n = 9) was measured. *B*: Shear rate in UCP1/DTA (n = 18) and controls (n = 14) was calculated by V_{mean} and vessel diameter. *C*: Leukocyte density (n = 41) and shear rate (n = 64) of all mice and days is plotted against blood glucose levels. Leukocyte density correlated positively linear to blood glucose values (R^2 = 0.96), whereas shear rate correlated negatively (P < 0.001) with a plateau phase at blood glucose values >160 mg/dl. Values are presented as means ± SE (*P < 0.05, **P < 0.01).

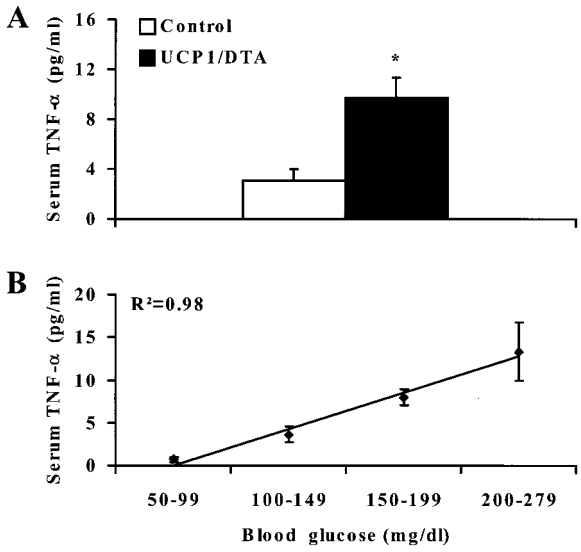

FIG. 8. A, TNF-α-Serum levels in UCP1/DTA ($n = 10$) and controls ($n = 12$). B, TNF-α-Serum levels of all mice ($n = 22$) is plotted against blood glucose values. TNF-α-Serum values showed a positive linear correlation to blood glucose levels ($R^2 = 0.98$).

VCAM-1, and ICAM-1) in a dose-dependent manner in human intestinal microvascular endothelial cells (35) and dermal endothelial cells (39). TNF-α mRNA levels in adipose tissue were reported to be increased in diabetic UCP1/DTA mice (14,40) similar to elevated plasma TNF-α found in obese humans (41). Furthermore, it has been shown that locally administered TNF-α increases LEI in subcutaneous tissue in vivo, without altering hemodynamic parameters (23). Our results show elevated TNF-α levels, which linearly correlate to glycemic levels ($R^2 = 0.98$), and can explain this further increase in LEI beyond the plateau phase of shear rate at glucose levels >160 mg/dl.

We have shown for the first time that functional and morpholocical microvascular alterations in subcutaneous tissue are present even at an early stage of diabetes. These microvascular parameters correlated with the metabolic situation represented by blood glucose levels and body weight. From our results, we conclude that even a short time of metabolic dysregulation causes not only functional but also morphological microvascular alterations. Therefore, a precise glycemic and metabolic control in patients can reduce diabetic angiopathies. To which extent patients with pathologic glucose tolerance and increased postprandial glucose levels suffer from microvascular alterations and the impact of other influencing factors (e.g., hyperinsulinemia and advanced glycation end products) on vascular deteriorations has to be further elucidated. To register early microvascular alterations, microvascular monitoring of patients with diabetes might be necessary to recognize early changes in microvascular properties (42). Our results support the growing evidence of the inflammatory component of diabetic disease and indicate that anti-inflammatory strategies might be beneficial to prevent microvascular deterioration. Further investigations must evaluate the benefit of such therapeutic strategies.

ACKNOWLEDGMENTS

This work was supported by a Werner Otto Stiftung research grant to N.H-A. and P.A. P.A. and A.H. were members of the DFG Graduate Kolleg [GRK336]. N.H.-A. and C.S. were members of the DFG Graduate Kolleg [GRK 476].

We thank M. Ammelt for help with the image processing analysis and Tim Padera for fruitful discussions and help with the manuscript.

REFERENCES

1. Carmeliet P: Mechanisms of angiogenesis and arteriogenesis. *Nat Med* 6:389–395, 2000
2. Haffner SM, Lehto S, Ronnemaa T, Pyorala K, Laakso M: Mortality from coronary heart disease in subjects with type 2 diabetes and in nondiabetic subjects with and without prior myocardial infarction. *N Engl J Med* 339:229–234, 1998
3. Stehouwer CD, Fischer HR, van Kuijk AW, Polak BC, Donker AJ: Endothelial dysfunction precedes development of microalbuminuria in IDDM. *Diabetes* 44:561–564, 1995
4. Antonetti DA, Lieth E, Barber AJ, Gardner TW: Molecular mechanisms of vascular permeability in diabetic retinopathy. *Semin Ophthalmol* 14:240–248, 1999
5. Panes J, Kurose I, Rodriguez-Vaca D, Anderson DC, Miyasaka M, Tso P, Granger DN: Diabetes exacerbates inflammatory responses to ischemia-reperfusion. *Circulation* 93:161–167, 1996
6. Lutty GA, Cao J, McLeod DS: Relationship of polymorphonuclear leukocytes to capillary dropout in the human diabetic choroid. *Am J Pathol* 151:707–714, 1997
7. Miyamoto K, Hiroshiba N, Tsujikawa A, Ogura Y: In vivo demonstration of increased leukocyte entrapment in retinal microcirculation of diabetic rats. *Invest Ophthalmol Vis Sci* 39:2190–2194, 1998
8. Chiarelli F, Santilli F, Mohn A: Role of growth factors in the development of diabetic complications. *Horm Res* 53:53–67, 2000
9. Koya D, King GL: Protein kinase C activation and the development of diabetic complications. *Diabetes* 47:859–866, 1998
10. Cheung AT, Ramanujam S, Greer DA, Kumagai LF, Aoki TT: Microvascular abnormalities in the bulbar conjunctiva of patients with type 2 diabetes mellitus. *Endocr Pract* 7:358–363, 2001
11. Lowell BB, S-Susulic V, Hamann A, Lawitts JA, Himms-Hagen J, Boyer BB, Kozak LP, Flier JS: Development of obesity in transgenic mice after genetic ablation of brown adipose tissue [see comments]. *Nature* 366:740–742, 1993
12. Cittadini A, Mantzoros CS, Hampton TG, Travers KE, Katz SE, Morgan JP, Flier JS, Douglas PS: Cardiovascular abnormalities in transgenic mice with reduced brown fat: an animal model of human obesity. *Circulation* 100:2177–2183, 1999
13. Hamann A, Busing B, Kausch C, Ertl J, Preibisch G, Greten H, Matthaei S: Chronic leptin treatment does not prevent the development of obesity in transgenic mice with brown fat deficiency. *Diabetologia* 40:810–815, 1997
14. Hamann A, Benecke H, Le Marchand-Brustel Y, Susulic VS, Lowell BB, Flier JS: Characterization of insulin resistance and NIDDM in transgenic mice with reduced brown fat. *Diabetes* 44:1266–1273, 1995
15. Klaus S, Munzberg H, Truloff C, Heldmaier G: Physiology of transgenic mice with brown fat ablation: obesity is due to lowered body temperature. *Am J Physiol* 274:R287–R293, 1998
16. Leunig M, Yuan F, Menger MD, Boucher Y, Goetz AE, Messmer K, Jain RK: Angiogenesis, microvascular architecture, microhemodynamics, and interstitial fluid pressure during early growth of human adenocarcinoma LS174T in SCID mice. *Cancer Res* 52:6553–6560, 1992
17. Hansen-Algenstaedt N, Stoll BR, Padera TP, Dolmans DE, Hicklin DJ, Fukumura D, Jain RK: Tumor oxygenation in hormone-dependent tumors during vascular endothelial growth factor receptor-2 blockade, hormone ablation, and chemotherapy. *Cancer Res* 60:4556–4560, 2000
18. Yuan F, Salehi HA, Boucher Y, Vasthare US, Tuma RF, Jain RK: Vascular permeability and microcirculation of gliomas and mammary carcinomas transplanted in rat and mouse cranial windows. *Cancer Res* 54:4564–4568, 1994
19. Lipowsky HH, Zweifach BW: Application of the "two-slit" photometric technique to the measurement of microvascular volumetric flow rates. *Microvasc Res* 15:93–101, 1978
20. Yuan F, Leunig M, Berk DA, Jain RK: Microvascular permeability of albumin, vascular surface area, and vascular volume measured in human

adenocarcinoma LS174T using dorsal chamber in SCID mice. *Microvasc Res* 45:269–289, 1993
21. Brizel DM, Klitzman B, Cook JM, Edwards J, Rosner G, Dewhirst MW: A comparison of tumor and normal tissue microvascular hematocrits and red cell fluxes in a rat window chamber model. *Int J Radiat Oncol Biol Phys* 25:269–276, 1993
22. Yuan F, Leunig M, Huang SK, Berk DA, Papahadjopoulos D, Jain RK: Microvascular permeability and interstitial penetration of sterically stabilized (stealth) liposomes in a human tumor xenograft. *Cancer Res* 54:3352–3356, 1994
23. Fukumura D, Salehi HA, Witwer B, Tuma RF, Melder RJ, Jain RK: Tumor necrosis factor alpha-induced leukocyte adhesion in normal and tumor vessels: effect of tumor type, transplantation site, and host strain. *Cancer Res* 55:4824–4829, 1995
24. Schroder S, Palinski W, Schmid-Schonbein GW: Activated monocytes and granulocytes, capillary nonperfusion, and neovascularization in diabetic retinopathy. *Am J Pathol* 139:81–100, 1991
25. Miyamoto K, Khosrof S, Bursell SE, Rohan R, Murata T, Clermont AC, Aiello LP, Ogura Y, Adamis AP: Prevention of leukostasis and vascular leakage in streptozotocin-induced diabetic retinopathy via intercellular adhesion molecule-1 inhibition. *Proc Natl Acad Sci U S A* 96:10836–10841, 1999
26. Antonetti DA, Barber AJ, Khin S, Lieth E, Tarbell JM, Gardner TW: Vascular permeability in experimental diabetes is associated with reduced endothelial occludin content: vascular endothelial growth factor decreases occludin in retinal endothelial cells: Penn State Retina Research Group. *Diabetes* 47:1953–1959, 1998
27. Mogensen CE, Christensen CK, Vittinghus E: The stages in diabetic renal disease with emphasis on the stage of incipient diabetic nephropathy. *Diabetes* 32 (Suppl. 2):64–78, 1983
28. Cheung AT, Perez RV, Chen PC: Improvements in diabetic microangiopathy after successful simultaneous pancreas-kidney transplantation: a computer-assisted intravital microscopy study on the conjunctival microcirculation. *Transplantation* 68:927–932, 1999
29. Kampfer H, Pfeilschifter J, Frank S: Expressional regulation of angiopoietin-1 and -2 and the tie-1 and -2 receptor tyrosine kinases during cutaneous wound healing: a comparative study of normal and impaired repair. *Lab Invest* 81:361–373, 2001
30. Holash J, Wiegand SJ, Yancopoulos GD: New model of tumor angiogenesis: dynamic balance between vessel regression and growth mediated by angiopoietins and VEGF. *Oncogene* 18:5356–5362, 1999
31. Rubanyi GM, Vanhoutte PM: Superoxide anions and hyperoxia inactivate endothelium-derived relaxing factor. *Am J Physiol* 250:H822–H827, 1986
32. von Andrian UH, Chambers JD, McEvoy LM, Bargatze RF, Arfors KE, Butcher EC: Two-step model of leukocyte-endothelial cell interaction in inflammation: distinct roles for LECAM-1 and the leukocyte beta 2 integrins in vivo. *Proc Natl Acad Sci U S A* 88:7538–7542, 1991
33. Von Andrian UH, Hansell P, Chambers JD, Berger EM, Torres Filho I, Butcher EC, Arfors KE: L-selectin function is required for beta 2-integrin-mediated neutrophil adhesion at physiological shear rates in vivo. *Am J Physiol*, 263:H1034–H1044, 1992
34. Booth G, Stalker TJ, Lefer AM, Scalia R: Elevated ambient glucose induces acute inflammatory events in the microvasculature: effects of insulin. *Am J Physiol Endocrinol Metab* 280:E848–E856, 2001
35. Haraldsen G, Kvale D, Lien B, Farstad IN, Brandtzaeg P: Cytokine-regulated expression of E-selectin, intercellular adhesion molecule-1 (ICAM-1), and vascular cell adhesion molecule-1 (VCAM-1) in human microvascular endothelial cells. *J Immunol* 156:2558–2565, 1996
36. Lawrence MB, Springer TA: Leukocytes roll on a selectin at physiologic flow rates: distinction from and prerequisite for adhesion through integrins. *Cell* 65:859–873, 1991
37. Schaffler A, Arndt H, Scholmerich J, Palitzsch K: Acute hyperglycemia causes severe disturbances of mesenteric microcirculation in an in vivo rat model. *Eur J Clin Invest* 28:886–893, 1998
38. Morigi M, Angioletti S, Imberti B, Donadelli R, Micheletti G, Figliuzzi M, Remuzzi A, Zoja C, Remuzzi G: Leukocyte-endothelial interaction is augmented by high glucose concentrations and hyperglycemia in a NF-kB-dependent fashion. *J Clin Invest* 101:1905–1915, 1998
39. Swerlick RA, Lee KH, Li LJ, Sepp NT, Caughman SW, Lawley TJ: Regulation of vascular cell adhesion molecule 1 on human dermal microvascular endothelial cells. *J Immunol* 149:698–705, 1992
40. Hamann A, Flier JS, Lowell BB: Decreased brown fat markedly enhances susceptibility to diet-induced obesity, diabetes, and hyperlipidemia. *Endocrinology* 137:21–29, 1996
41. Dandona P, Weinstock R, Thusu K, Abdel-Rahman E, Aljada A, Wadden T: Tumor necrosis factor-alpha in sera of obese patients: fall with weight loss. *J Clin Endocrinol Metab* 83:2907–2910, 1998
42. Groner W, Winkelman JW, Harris AG, Ince C, Bouma GJ, Messmer K, Nadeau RG: Orthogonal polarization spectral imaging: a new method for study of the microcirculation. *Nat Med* 5:1209–1212, 1999